ADVANCED OPTICAL MATERIALS
www.advopticalmat.de

Reconfigurable Digital Metamaterial for Dynamic Switching of Terahertz Anisotropy

*Prakash Pitchappa, Chong Pei Ho, Longqing Cong, Ranjan Singh, Navab Singh, and Chengkuo Lee**

Terahertz (THz) regime of the electromagnetic (EM) spectrum lies between the microwave and infrared regions (f = 0.1–10 THz). THz wave combines the merits of both these neighboring spectral regions and potentially enables numerous impactful applications such as noninvasive medical inspection, nondestructive fault analysis, security surveillance, and next-generation high-speed wireless communication networks.[1–4] However, THz wave interacts minimally with naturally occuring materials and this has hindered the development of devices for THz wave manipulation.[5] Metamaterials offer the possibility to realize EM properties for desired spectral range and has significantly bridged the so-called "THz gap". Metamaterial is an array of subwavelength structures, whose properties can be engineered through the design of unit cell geometry. The diversity of the unit cell shape along with the scalability has led to the demonstration of even exotic THz properties such as artificial magnetism,[6] negative refractive index,[7,8] unnaturally large refractive index,[9] chirality,[10] polarization control,[11] wavelength selective absorption,[12,13] electromagnetically induced transparency analogue,[14,15] and slow light behavior.[16] Furthermore, the THz properties realized through metamaterials can also be actively controlled through external stimuli. This tunability in metamaterial response adds in a new dimension for the manipulation of THz wave. Tunable metamaterials are reported for the active control of varied THz properties such as magnetic resonance,[17–23] electrical resonance,[23–28] polarization response,[29–31] chirality,[32] absorption,[33–35] multiband and broadband modulation,[36–42] and near-field coupled resonances.[43–45] Recently, digital metamaterials, coding metamaterials, and programming metamaterials have been demonstrated,[46–51] where discrete subwavelength unit cells with specific geometrical filling ratio act as "digital bits." The state of these metabits are defined by their reflection phases at a given frequency. The metamaterial then formed by placing these metabits in a coding sequence determines the phase gradient of the metamaterial and hence the reflection profile of incident EM waves. By changing the coding sequence, the reflection beam can be steered along specific direction with a desired reflection profile.[49–51]

From an alternate perspective, the metabit states can also be defined based on the transmission intensity rather than the reflection phase. These metamaterials can be considered as a new class of coding metamaterials, which enable advanced resonance-based EM wave manipulation. More interestingly, a single metabit can be switched between ON and OFF states, i.e., transmission high (or no resonance) and transmission low (or presence of resonance), respectively through external stimulus at a given frequency. This allows for the dynamic selection of the functionality of the coding metamaterial based on the state of the metabits. The dynamically switchable metabit can be realized using various control mechanism such as optical,[17,24] magnetic,[18] or thermal stimulus.[19] However, above-mentioned control mechanisms do not allow for selective control of active elements integrated into the unit cell geometry and hence provides only single metabit system. In order to realize multibit resonance-based metamaterial, independent control of active elements integrated into a single unit cell is highly desirable. Microelectromechanical system (MEMS)-based metamaterials by integrating microactuators into the unit cell geometry are reported to achieve isolation of control at the unit cell level.[52] Especially, the out-of-plane deformable microactuators-based metamaterials are of great interest, owing to its simplicity in design and versatility in application. Multiple microcantilevers can be readily integrated to the unit cell geometry and upon electrical isolation will readily enable dynamically reconfigurable multibit digital metamaterial for advanced manipulation of THz waves. These multibit digital metamaterials pave way for the realization of disruptive THz functional devices such as multifunctional and programmable metamaterials. The multifunctional metamaterial will provide independent control of multiple THz properties by integrating various resonator designs into a single metamaterial. On the other hand, programmable metamaterial can be realized by controlling identical unit cells individually and then dynamically programmed

P. Pitchappa, C. P. Ho, Prof. C. Lee
Department of Electrical & Computer Engineering
National University of Singapore
Singapore 117576, Singapore
E-mail: elelc@nus.edu.sg
P. Pitchappa, C. P. Ho, Prof. C. Lee
Center for Intelligent Sensors and MEMS
National University of Singapore
Singapore 117576, Singapore
P. Pitchappa, C. P. Ho, N. Singh
Institute of Microelectronics
Agency for Science, Technology, and Research (A*STAR)
11 Science Park Road, Singapore Science Park II,
Singapore 117685, Singapore
L. Cong, Prof. R. Singh
Division of Physics and Applied Physics
Centre for Disruptive Photonic Technologies
School of Physical and Mathematical Sciences
Nanyang Technological University
Singapore 637371, Singapore

DOI: 10.1002/adom.201500588

to function as a tunable filter, switchable polarizers, spatial light modulator, phase gradient metamaterial, or even a random metamaterial.

Active control of THz anisotropy is a critical EM parameter that will enable numerous THz polarimetric devices such as active wave plates, beam splitters, and isolators for application in THz spectroscopy, ellipsometry, and imaging systems. Active metamaterials for dynamic switching of linear polarization response from either *x*- or *y*-polarization to polarization-insensitive state at a given frequency are reported before.[17,29,30] In order to get complete control of anisotropy it is critical to achieve symmetry breaking of the metamaterial unit cell geometry independently along *x*- and *y*-directions. In this report, a digital metamaterial for independent control of orthogonal polarization response of the THz waves is experimentally demonstrated. Two orthogonally placed, out-of-plane deformable, electrically isolated microcantilevers allow for the independent switching of linear polarization responses in the THz spectral region. The physical position of the microcantilevers defines the state of the cantilevers and can be dynamically switched between OFF and ON states by applying voltage across the cantilevers and Si substrate. When the cantilever is suspended with an air gap the state is defined as "OFF" or "0" state and the state in which the cantilever is in physical contact with the substrate is defined as "ON" or "1" state. As the two cantilevers are electrically isolated, the state of the metamaterial is defined as S_{XY}, where "x" represents the state of the MCX cantilever, which is placed along the *x*-direction, and "y" represents the state of MCY cantilever, which is placed along the y direction. The MCX and MCY cantilevers dominantly influences the resonance features of the metamaterial for *x*-polarized (electric field along *x*-direction) and *y*-polarized (electric field along *y*-direction) THz incidence, respectively. Hence, for *x*-polarized incidence, the resonance at 0.8 THz can be controlled by reconfiguring the digital metamaterial between S_{0Y} and S_{1Y} and similarly for *y*-polarized incidence the reconfiguration of states between S_{X0} and S_{X1} provides the dynamic control of the resonance at 0.8 THz. The anisotropy of the proposed digital metamaterial can be actively switched from less than unity to 2.65 at 0.8 THz though selective reconfiguration of these microcantilevers. The proposed approach can be potentially scaled to integrate more number of independently controlled cantilevers for complex multibit coding metamaterials and higher degree of polarization control.

The unit cell of the proposed digital metamaterial consists of four geometrically identical microcantilevers placed with Π/2 rotational symmetry. Length of each cantilever (cl) is 34 µm, length of tip (tl) is 20 µm, and width (cw) is 3 µm. Two cantilevers, FCX and MCX are placed facing each other along the *x*-direction, while the other two cantilevers, FCY and MCY are placed along the *y*-direction as shown in **Figure 1**a. The FCX and FCY cantilevers are fixed to the Si substrate at all times, while the MCX and MCY cantilevers are released and are movable. The microcantilevers are suspended bimorph structures made of 500 nm aluminum (Al) over 50 nm aluminum oxide (Al_2O_3) dielectric layer, fabricated on lightly doped silicon (Si) substrate.[28] Silicon-di-oxide is used as the sacrificial layer and the MCX and MCY cantilevers are released using vapor hydrofluoric acid. When released, the MCX and MCY cantilevers curve up in the out-of-plane direction due to the residual stress gradient in the bimaterial layers. The optical image (OM) of the fabricated metamaterial after the release step is shown in **Figure 2**a and the scanning electron microscope (SEM) image of the metamaterial unit cell is shown in Figure 2b, respectively. The digital holographic microscope (DHM) image shows a quantitative description of the release height as gradual change in phase from anchor to the tip position as shown in Figure 2c. The initial tip displacement of the released MCX (red curve) and MCY cantilevers (blue curve) was measured to be $g \approx 3$ µm as shown in Figure 2d. The small mismatch between the release height of MCX and MCY cantilevers is attributed to the fabrication imperfections in the devices.

To reconfigure the physical position of movable cantilevers, voltage is applied across the released cantilever and Si substrate. The applied voltage generates an attractive electrostatic force, which deforms the movable cantilever towards the fixed substrate. This physical deformation in cantilevers will bring in an opposing force called the spring restoring force. The balance between the electrostatic force and restoring force determines the final position of the cantilever for any given voltage. However, the electrostatic force increases sharply relative to the restoring force when the voltage is increased. After a critical value of applied voltage called the "pull-in voltage" (≈30 V), electrostatic force will be higher than the restoring force and therefore will completely close the air gap between the cantilever and Si substrate.[53–55] The cantilever acts as a mechanical switch that can be in one of the two states based on the physical position of the released cantilever and voltage applied. The "OFF" (or "0") state is the state in which the cantilevers are released and no voltage is applied, while the "ON" (or "1") state refers to the situation where the cantilever is physically in contact with Si substrate when the applied voltage is higher than the pull-in voltage of 30 V. Figure 2d shows the measured out-of-plane deformation profile for the MCX (orange curve) and MCY cantilevers (green curve) in ON state. The flat profile of the cantilevers confirms the physical contact of cantilevers on the Si substrate. The negative 100 nm displacement measured in the ON state for both cantilevers represents the sacrificial layer thickness, which is removed during the release process. The MCX cantilevers in all the metamaterial unit cells are electrically connected to each other through metal interconnects, but is isolated from the metal line connecting all the MCY cantilevers in the metamaterial. This electrical isolation allows for the independent actuation of MCX and MCY cantilevers. The MCX and MCY cantilevers forms the digital bits, which can be dynamically switched to achieve desired transmission response for *x*- and *y*-polarized incidence THz wave at a given frequency. Based on the physical position the digital metamaterial can be in one of four possible states—MCX-OFF/MCY-OFF (S_{00}), MCX-ON/MCY-OFF (S_{10}), MCX-OFF/MCY-ON (S_{10}), and MCX-ON/MCY-ON (S_{11}) as schematically shown in Figure 1b,c,d, and e, respectively.

The digital metamaterial is characterized using THz time-domain spectroscopy in transmission mode for normally incident THz waves with predefined *x*-polarization (electric field is along the FCX-MCX cantilever direction or *x*-direction) or *y*-polarization (electric field is along the FCY-MCY cantilever direction or *y*-direction) as shown in Figure 1a. The simulated

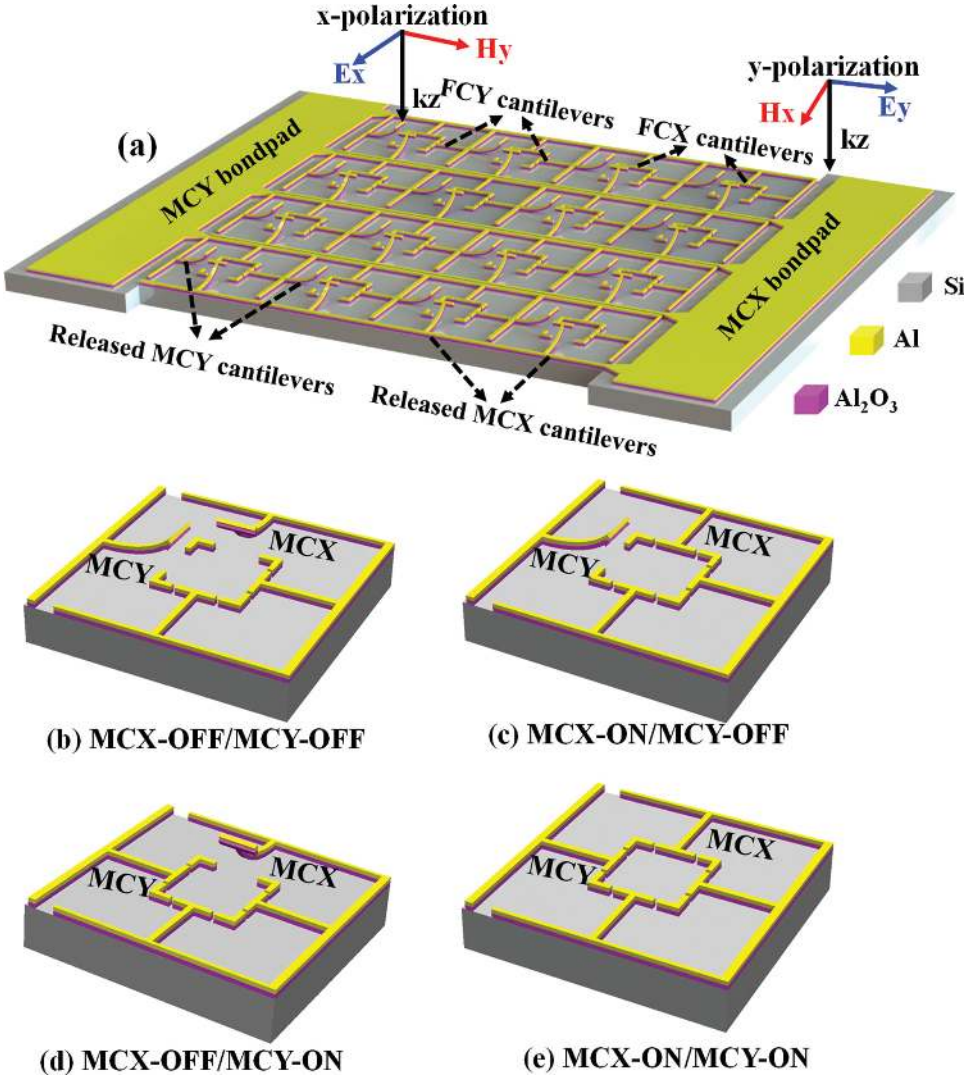

Figure 1. Schematic drawing of the proposed digital metamaterial and various reconfiguration states. a) Digital metamaterial formed by two independently reconfigurable cantilevers—MCX and MCY. The orthogonal placement allows for switching the linear polarization response of the metamaterial dynamically. The isolated electrical control of MCX and MCY cantilevers allows for four possible reconfiguration states. The schematics of the unit cell in each state is shown in b) MCX-OFF/MCY-OFF, c) MCX-ON/MCY-OFF, d) MCX-OFF/MCY-ON, and e) MCX-ON/MCY-ON.

transmission spectra of the digital metamaterial for *x*-polarization incidence with MCX cantilever in OFF and ON states, while the MCY cantilever is kept in ON state are shown in in **Figure 3**a. When the MCX cantilever is in OFF state, the simulated transmission spectrum (red-circle curve) of the metamaterial in S_{01} state shows two distinct resonances at 0.724 and 0.886 THz. The surface current distribution at 0.724 THz is shown in Figure 3c and it can be observed that there is a strong current induced in the FCX cantilever and a weaker current in the MCX-OFF cantilever. The reduction in current is caused due to the air gap beneath the MCX-OFF cantilevers compared to the FCX cantilever that is in direct contact with Si substrate. The FCX and MCX-OFF cantilevers effectively act as two separate single resonators. However, at 0.886 THz, there is only a weak current induced in the MCX-OFF cantilever as shown in Figure 3d, which acts as an independent resonator. This causes the resonance to be at a higher frequency owing to the reduced effective dimension of the resonator.[28] It is important to note that the metal lines along with a small in-plane gap contributes to the resonances and the in-plane gap is unavoidable due to the desired electrical isolation between MCX and MCY cantilevers. When the MCX cantilever is switched to ON state, the simulated transmission spectrum (green-square curve) has a single resonance at 0.644 THz. As the MCX cantilever is switched ON, the air gap is drastically reduced, thereby causing the effective capacitance of the resonator to increase and lowering the resonant frequency. Strong and identical surface currents are induced in both FCX and MCX-ON cantilevers at 0.644 THz. The measured transmission spectra for metamaterial in S_{01} state (red-circle curve) and S_{11} state (green-square curve) shown in Figure 2b matches quite well with the simulated results. In S_{01} state, there are two distinct resonances at 0.64 and 0.8 THz and for S_{11} state, a single resonance is observed at 0.675 THz. The small mismatch between the simulated and measured

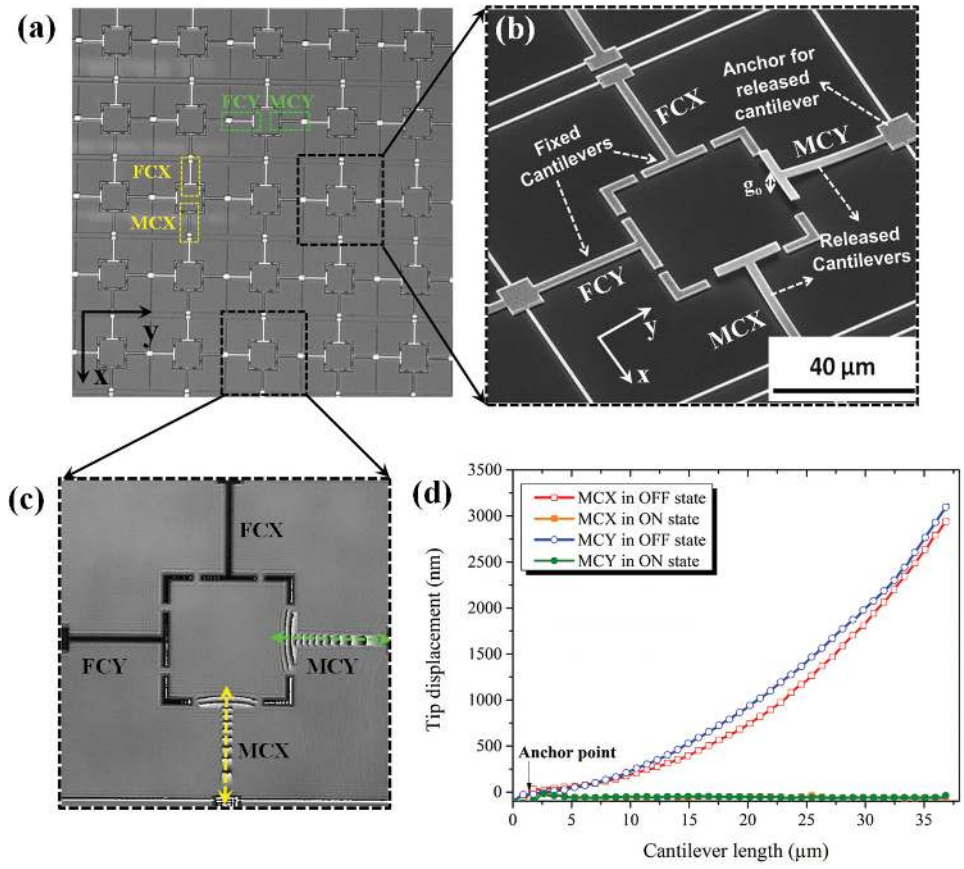

Figure 2. Fabricated digital metamaterial after release step. a) Microscopic image of the metamaterial with MCX and MCY cantilevers in OFF state. The out-of-plane displacement of the released MCX and MCY cantilevers can be quantitatively observed from the out-of-focus, relative to the FCX and FCY cantilevers, which is completely in focus. b) Scanning electron microscope image of the unit cell with MCX and MCY in OFF state and the air gap between the MCX, MCY cantilevers and Si substrate can be clearly observed. c) R-DHM phase profile of the corresponding unit cell, d) Measured out-of-plane deformation of the MCX cantilevers in OFF state (red-hollow square) and ON state (orange-solid square) and MCY cantilever in OFF state (blue-hollow circle) and ON state (green-solid circle), respectively.

spectra can be attributed to the variation in the geometrical parameters and the deviation of the material properties used in simulation from the real case. The position of MCY cantilever has minimal influence on the resonance spectra of the digital metamaterial for *x*-polarization incidence (see Supporting Information for more details). Hence, for the *x*-polarization incidence, the resonance at 0.8 THz is selectively switched by controlling the state of MCX cantilever.

The rotational symmetry of the metamaterial allows for similar response for the *y*-polarization incidence (the electric field is along the FCY-MCY cantilever direction and perpendicular to FCX-MCX cantilevers). Now, the state of the MCY cantilever predominantly determines the resonance behavior of the digital metamaterial. The simulated transmission spectra of the metamaterial with MCY cantilever in OFF and ON states with MCX cantilever in ON state, for *y*-polarization incidence are shown in **Figure 4**a. When the MCY cantilevers are in OFF state, the simulated transmission spectrum (black-circle curve) shows two distinct resonances at 0.736 THz and 0.84 THz. The current distribution at 0.736 THz and 0.84 THz are shown in Figure 4c,d, respectively and is identical to the MCX case but rotated by 90°. Hence, the resonance mechanisms at the resonant frequencies are similar to the *x*-polarized incidence. When the MCY cantilever is switched to ON state, there is only a single resonance at 0.61 THz as shown in simulated spectra of the metamaterial in S_{11} state (blue-square curve) in Figure 4a. The strong current induced in the FCY-MCY-ON cantilevers shown in Figure 4e confirms the excitation of a single-dipole-mode resonance across the entire length of MCY-FCY cantilever configuration. The measured transmission spectra for *y*-polarized incidence show two resonance dips at 0.64 THz and 0.8 THz for S_{10} state (black-circle curve) and a single resonance at 0.65 THz for S_{11} state (blue-square curve), respectively, as shown in Figure 4b. Compared to the *x*-polarization excitation, the influence of the metal interconnects is highly reduced as there is no in-plane gap along the *y*-direction in the unit cell geometry. The slight mismatch in the resonant frequencies for *x*-polarization and *y*-polarization incidence at different configuration states is caused due to the lack of perfect rotational symmetry in the metamaterial unit cell, as the need for isolation between metal lines is inevitable for providing the independent control for MCX and MCY cantilevers.

The isolated control of MCX and MCY cantilevers allows for the breaking and recovery of the rotational symmetry in the

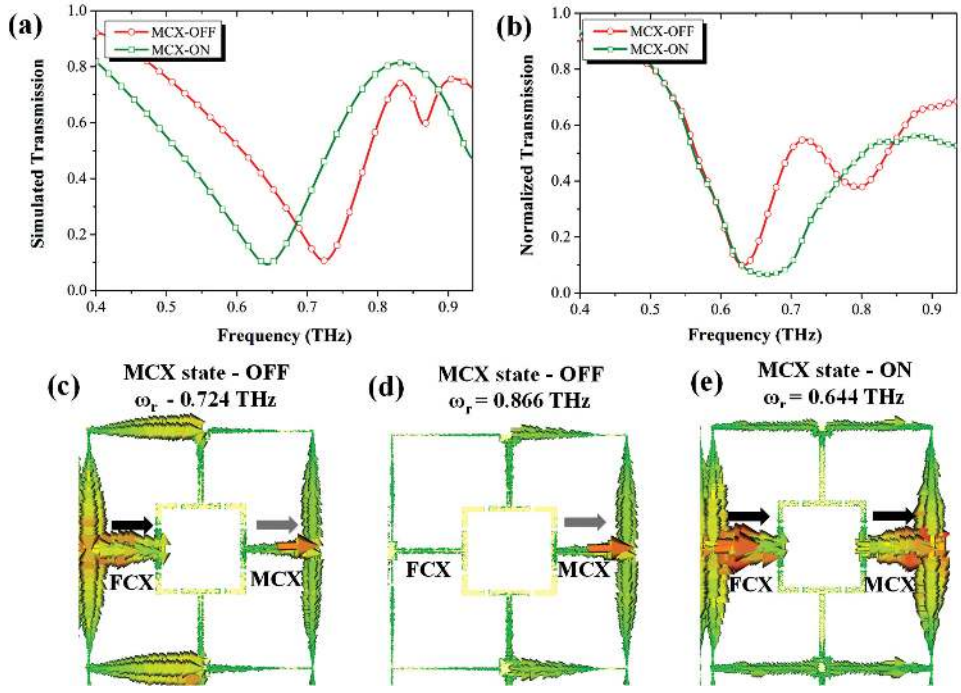

Figure 3. *x*-polarization response of digital metamaterial. a) Simulated and b) Measured transmission spectra of the metamaterial for *x*-polarization incidence (electric field along FCX-MCX cantilever direction) with MCX cantilevers in OFF state (red-circle) and ON state (green-square), respectively. Simulated surface current distribution of the metamaterial with MCX in OFF state at c) 0.724 THz and d) 0.886 THz and e) with MCX in ON state at 0.644 THz, respectively.

metamaterial unit cell on demand and hence provides dynamic switching of THz anisotropy. The anisotropy (A) of the metamaterial is defined as the ratio of transmission response of the metamaterial for *x*-polarization and *y*-polarization of incident THz waves. That is $A = T_X/T_Y$, where T_X and T_Y are the transmission intensities of the digital metamaterial for *x*-polarization and *y*-polarization of THz waves, respectively, and is shown in **Figure 5**. At 0.8 THz for MCX-OFF and MCY-ON state, resonance is observed for *x*-polarization incidence (low transmission T_X), but no resonance occurs for *y*-polarization incidence (high transmission, T_Y). Hence, the calculated anisotropy is 2.65 at 0.8 THz. When the MCX cantilever is switched to ON state, the resonance at 0.8 THz disappears and hence the anisotropy is almost unity due to the high transmission for *x*- and *y*-polarization incidence as shown from the red-triangle curve in Figure 5. Similarly, when MCY is in OFF state, the resonance occurs for *y*-polarization incidence and hence the anisotropy is approximately 0.8 at 0.8 THz. Thus, the proposed approach of independent reconfiguration of MCX and MCY cantilevers has the power to dynamically switch the anisotropy of the metamaterial between less and more than unity values at any desired frequency. The nonunity value for measured anisotropy when both MCX and MCY cantilevers are in ON state and the mismatch between the values of anisotropy for MCX switching and MCY switching cases is primarily caused by the asymmetry due to the metal interconnects. This can be overcome by having bimetallic layers, where in one metal layer the *x*-polarization-responsive resonators can be formed, while the other metal layer houses the *y*-polarization-responsive resonators. These two isolated metal layers can be designed to form a perfectly symmetric unit cell geometry. Furthermore, the proposed digital metamaterial can be scaled up to have more number of cantilevers that could be independently controlled to provide even more flexibility in manipulating the THz anisotropy. Switchable phase gradient metamaterial is an interesting prospective work of digital MEMS metamaterial. For instance, the phase of the metamaterial can be designed by gradually varying the release length and tip displacement of the microcantilevers. Hence in the OFF state, the metamaterial will enable desired phase gradient. However, when the release part of the cantilevers is switched to ON state, all the unit cells will be geometrically identical and will extinguish the gradient in the metamaterial. These actively phase-controlled metamaterial can further enable numerous interesting applications such as switchable quarter wave plate, beam isolators, and tunable THz lens.

In summary, digital metamaterial with selectively reconfigurable microcantilevers integrated into a single unit cell for independent control of orthogonal THz polarization response is experimentally demonstrated. The switching of MCX cantilevers controls the *x*-polarization response, while MCY cantilevers provides selective resonance switching only for *y*-polarization incidence, respectively. Hence, the proposed metamaterial can be actively reconfigured to interact only with *x*-polarized or only *y*-polarized incidence or both *x*- and *y*-polarized incidence or neither *x*- nor *y*-polarization of incidence THz waves at 0.8 THz. This allows for dynamic switching of THz anisotropy between values less than unity(0.8), equal to unity or more than unity (2.65) at 0.8 THz. This advanced control over

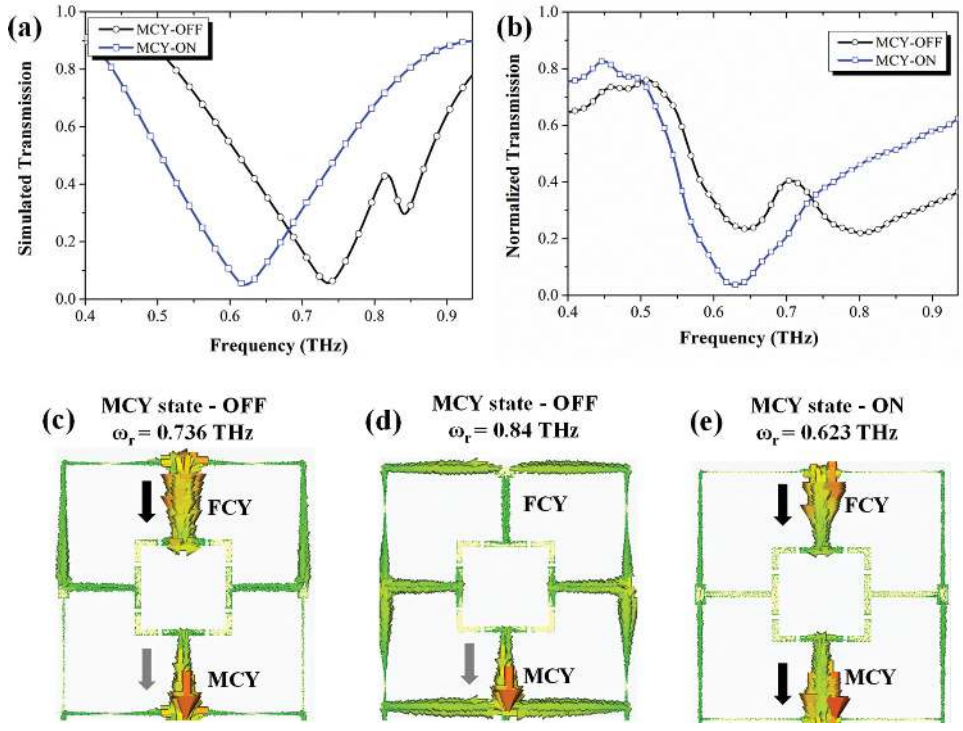

Figure 4. *y*-polarization response of digital metamaterial. a) Simulated and b) measured transmission spectra of the metamaterial for *y*-polarization incidence (electric field along FCY-MCY cantilever direction) with MCY cantilevers in OFF state (black-circle) and ON state (blue-square), respectively. Simulated surface current distribution of the metamaterial with MCY in OFF state at c) 0.736 THz and d) 0.84 THz, and e) with MCY in ON state at 0.623 THz, respectively.

polarization response of metamaterial will enable the realization of numerous high-performance polarimetric devices to be used in the next-generation high-speed communication systems operating at sub-THz regime and THz spectroscopy. The proposed class of digital metamaterial with multibit configuration is a key technological milestone for the realization of disruptive advanced THz materials such as multifunctional metamaterials and programmable metamaterials, which can be dynamically transformed to take up one of many functional forms such as tunable filter, spatial light modulator, gradient metamaterials, or a random metamaterial.

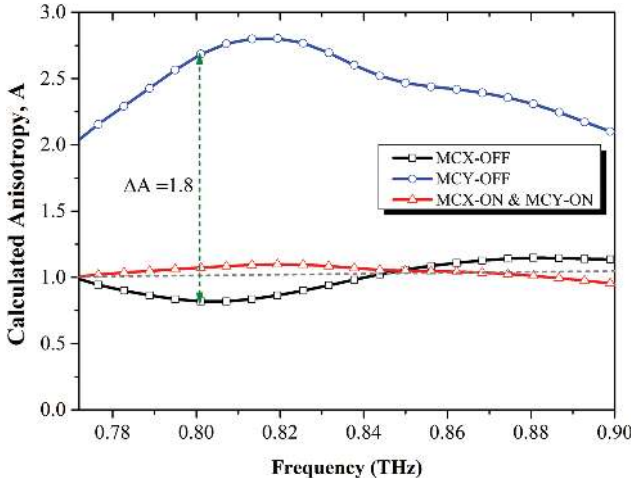

Figure 5. Calculated anisotropy of the digital metamaterial when MCX cantilever is in OFF state (black-square), MCY cantilever is in OFF state (blue-circle) and both MCX and MCY cantilevers in ON state (red-triangle), respectively.

Experimental Section

Electromechanical Characterization: The deflection profile of released microcantilevers was measured using Lyncee Tec. reflection digital holographic microscope (R-DHM). The released chips were wire bonded to a printed circuit board (PCB). Separate voltage supply was used for the actuation of MCX and MCY cantilevers. Si substrate was chosen as the ground potential, and the microcantilevers were positively biased. The voltage was increased between the microcantilevers and Si substrate and when the applied voltage was higher than the pull-in voltage (≈30 V), the microcantilevers come in physical contact with the Si substrate. The pull-in could be clearly observed through the optical microscope fitted on the R-DHM. The Al_2O_3 layer beneath the Al layer ensured that there was no current flowing from Al layer to Si substrate, when pull-in occurred. This is crucial because if the current flows through the Al/Si junction, then the temperature will raise up locally thereby melting the Al tips with the Si substrate, and will permanently damage the device.

Electromagnetic Characterization: THz time-domain spectroscopy (THz-TDS) was used to characterize the transmission spectra of the metamaterial at different configuration states. THz wave was incident normally to the sample with predetermined polarization (*x*-polarization or *y*-polarization). The released metamaterial chip was bonded to a PCB with a hole of 1 cm × 1 cm in center. The bonded sample was then placed in the nitrogen-filled chamber. The MCX bondpad and MCY bondpad were connected to two different voltage sources. Si substrate was kept as ground, while positive potential was applied to

MCX and MCY bondpads. The transmission spectra was measured at different reconfiguration states for both *x*-polarization and *y*-polarization incidence. The measured data was then normalized with transmission through bare Si substrate of same thickness as the samples.

Supporting Information

Supporting Information is available from the Wiley Online Library or from the author.

Acknowledgements

The authors acknowledge the financial support from research grant of AcRF Tier 2-MOE2012-T2-2-154 at the National University of Singapore and National Natural Science Foundation of China (Grant No. 61474078) at National University of Singapore Suzhou Research Institute (NUSRI), Suzhou, China.

Received: October 12, 2015
Revised: November 13, 2015
Published online: December 16, 2015

[1] P. H. Seigel, *IEEE Trans. Microwave Theory Tech.* **2004**, *52*, 10.
[2] M. Tonouchi, *Nat. Photonics* **2007**, *1*, 2.
[3] C. Yu, S. Fan, Y. Sun, E. P. MacPherson, *Quant. Imaging Med. Surg.* **2012**, *2*, 1.
[4] S. Koenig, D. Lopez-Diaz, J. Antes, F. Boes, R. Henneberger, A. Leuther, A. Tessmann, R. Schmogrow, D. Hillerkuss, R. Palmer, T. Zwick, C. Koos, W. Freude, O. Ambacher, J. Leuthold, I. Kallfass, *Nat. Photonics* **2013**, *7*, 12.
[5] C. Sirtori, *Nature* **2002**, *417*, 6885.
[6] T. J. Yen, W. J. Padilla, N. Fang, D. C. Vier, D. R. Smith, J. B. Pendry, D. N. Basov, X. Zhang, *Science* **2004**, *5663*, 303.
[7] S. Zhang, Y. S. Park, J. Li, X. Lu, W. Zhang, X. Zhang, *Phys. Rev. Lett.* **2009**, *102*, 023901.
[8] O. Paul, C. Imhof, B. Reinhard, R. Zengerle, R. Beigang, *Opt. Express* **2009**, *16*, 9.
[9] M. Choi, S. H. Lee, Y. Kim, S. B. Kang,J. Shin, M. H. Kwak, K. Y. Kang, Y. H. Lee, N. Park, B. Min, *Nature* **2011**, *470*, 7334.
[10] J. Zhou, D. R. Chowdhury, R. Zhao, A. K. Azad, H. T. Chen, C. M. Soukoulis, A. J. Taylor, J. F. O'Hara, *Phys. Rev. B* **2012**, *86*, 035448.
[11] L. Cong, N. Xu, W. Zhang, R. Singh, *Adv. Opt. Mater.* **2015**, *3*, 9.
[12] H. Tao, N. I. Landy, C. M. Bingham, X. Zhang, R. D. Averitt, W. J. Padilla, *Opt. Express* **2008**, *16*, 10.
[13] N. I. Landy, C. M. Bingham, T. Tyler, N. Jokerst, D. R. Smith, W. J. Padilla, *Phys. Rev. B* **2009**, *79*, 125104.
[14] S. Y. Chiam, R. Singh, C. Rockstuhl, F. Lederer, W. Zhang, A. A. Bettiol, *Phys. Rev. B* **2009**, *80*, 153103.
[15] R. Singh, C. Rockstuhl, F. Lederer, W. Zhang, *Phys. Rev. B* **2009**, *79*, 085111.
[16] M. Manjappa, S. Y. Chiam, L. Cong, A. A. Bettiol, W. Zhang, R. Singh, *Appl. Phys. Lett.* **2015**, *106*, 181101.
[17] W. J. Padilla, A. J. Taylor, C. Highstrete, M. Lee, R. D. Averitt, *Phys. Rev. Lett.* **2006**, *96*, 107401.
[18] H. Němec, P. Kužel, F. Kadlec, C. Kadlec, R. Yahiaoui, P. Mounaix, *Phys. Rev. B* **2009**, *79*, 241108.
[19] H. Tao, A. C. Strikwerda, K. Fan, W. J. Padilla, X. Zhang, R. D. Averitt, *Phys. Rev. Lett.* **2009**, *103*, 147401.
[20] W. M. Zhu, A. Q. Liu, X. M. Zhang, D. P. Tsai, T. Bourouina, J. H. Teng, X. H. Zhang, H. C. Guo, H. Tanoto, T. Mei, G. Q. Lo, D. L. Kwong, *Adv. Mater.* **2011**, *23*, 15.
[21] Z. Liu, C. Y. Huang, H. Liu, X. Zhang, C. Lee, *Opt. Express* **2013**, *21*, 5.
[22] Y. S. Lin, Y. Qian, F. Ma, Z. Liu, P. Kropelnicki, C. Lee, *Appl. Phys. Lett.* **2013**, *102*, 11.
[23] Z. Han, K. Kohno, H. Fujita, K. Hirakawa, H. Toshiyoshi, *Opt. Express* **2014**, *22*, 18.
[24] H. T. Chen, W. J. Padilla, J. M. O. Zide, A. C. Gossard, A. J. Taylor, R. D. Averitt, *Nature* **2006**, *444*, 7119.
[25] H. T. Chen, W. J. Padilla, M. J. Cich, A. K. Azad, R. D. Averitt, A. J. Taylor, *Nat. Photonics* **2009**, *3*, 3.
[26] F. Ma, Y. Qian, Y. S. Lin, H. Liu, X. H. Zhang, Z. Liu, J. M. L. Tsai, C. Lee, *Appl. Phys. Lett.* **2012**, *102*, 16.
[27] F. Ma, Y. S. Lin, X. H. Zhang, C. Lee, *Light: Sci. Appl.* **2014**, *3*, e171.
[28] P. Pitchappa, C. P. Ho, L. Dhakar, Y. Qian, N. Singh, C. Lee, *J. Microelectromech. Syst.* **2015**, *24*, 3.
[29] W. M. Zhu, A. Q. Liu, W. Zhang, J. F. Tao, T. Bourouina, J. H. Teng, X. H. Zhang, Q. Y. Wu, H. Tanoto, H. C. Guo, G. Q. Lo, D. L. Kwong, *Appl. Phys. Lett.* **2011**, *99*, 22.
[30] W. M. Zhu, A. Q. Liu, T. Bourouina, D. P. Tsai, J. H. Teng, X. H. Zhang, G. Q. Lo, D. L. Kwong, N. I. Zheludev, *Nat. Commun.* **2012**, *3*, 1274.
[31] W. Zhang, W. M. Zhu, J. M. Tsai, G. Q. Lo, D. L. Kwong, E. P. Li, A. Q. Liu, presented at *IEEE 26th Int. Conf. Micro Electro Mechanical Systems (MEMS)*, Taipei, January **2013**.
[32] S. Zhang, J. Zhou, Y. S. Park, J. Rho, R. Singh, S. Nam, A. K. Azad, H. T. Chen, X. Yin, A. J. Taylor, X. Zhang, *Nat. Commun.* **2012**, *3*, 7.
[33] D. Shrekenhamer, W. C. Chen, W. J. Padilla, *Phys. Rev. Lett.* **2013**, *110*, 177403.
[34] D. Shrekenhamer, J. Montoya, S. Krishna, W. J. Padilla, *Adv. Opt. Mater.* **2013**, *1*, 12.
[35] H. R. Seren, G. R. Keiser, L. Cao, J. Zhang, A. C. Strikwerda, K. Fan, G. D. Metcalfe, M. Wraback, X. Zhang, R. D. Averitt, *Adv. Opt. Mater.* **2014**, *2*, 12.
[36] N. H. Shen, M. Kafesaki, T. Koschny, L. Zhang, E. N. Economou, C. M. Soukoulis, *Phys. Rev. B* **2009**, *79*, 161102.
[37] P. Pitchappa, C. P. Ho, L. Dhakar, C. Lee, *Optica* **2015**, *2*, 6.
[38] M. Liu, H. Y. Hwang, H. Tao, A. C. Strikwerda, K. Fan, G. R. Keiser, A. J. Sternbach, K. G. West, S. Kittiwatanakul, J. Lu, S. A. Wolf, F. G. Omenetto, X. Zhang, K. A. Nelson, R. D. Averitt, *Nature* **2012**, *487*, 7407.
[39] C. P. Ho, P. Pitchappa, Y. S. Lin, C. Y. Huang, P. Kropelnicki, C. Lee, *Appl. Phys. Lett.* **2014**, *104*, 16.
[40] P. Pitchappa, C. P. Ho, Y. S. Lin, P. Kropelnicki, C. Y. Huang, N. Singh, C. Lee, *Appl. Phys. Lett.* **2014**, *104*, 15.
[41] M. Unlu, M. R. Hashemi, C. W. Berry, S. Li, S. H. Yang, M. Jarrahi, *Sci. Rep.* **2014**, *4*, 5708.
[42] P. Pitchappa, C. P. Ho, Y. Qian, L. Dhakar, N, Singh, C. Lee, *Sci. Rep.* **2015**, *5*, 11678.
[43] J. Gu, R. Singh, X. Liu, X. Zhang, Y. Ma, S. Zhang, S. A. Maier, Z. Tian, A. K. Azad, H. T. Chen, A. J. Taylor, J. Han, W. Zhang, *Nat. Commun.* **2012**, *3*, 1151.
[44] D. R. Chowdhury, R. Singh, A. J. Taylor, H. T. Chen, A. K. Azad, *Appl. Phys. Lett.* **2013**, *102*, 011122.
[45] F. Miyamaru, H. Morita, Y. Nishiyama, T. Nishida, T. Nakanishi, M. Kitano, M. W. Takeda, *Sci. Rep.* **2014**, *4*, 4346.
[46] C. D. Giovampaola, N. Engheta, *Nat. Mater.* **2014**, *13*, 12.
[47] J. Wang, W. B. Lu, J. L. Liu, T. J. Cui, *Plasmonics* **2015**, *10*, 5.
[48] T. J. Cui, M. Q. Qi, X. Wan, J. Zhao, Q. Cheng, *Light: Sci. Appl.* **2014**, *3*, e218.
[49] L. Liang, M. Qi, J. Yang, X. Shen, J. Zhai, W. Xu, B. Jin, W. Liu, Y. Feng, C. Zhang, H. Lu, H. T. Chen, L. Kang, W. Xu, J. Chen, T. J. Cui, P. Wu, S. Liu, *Adv. Opt. Mater.* **2015**, DOI: 10.1002/adom.201500206.
[50] D. S. Dong, J. Yang, Q. Cheng, J. Zhao, L. H. Gao, S. J. Ma, S. Liu, H. B. Chen, Q. He, W. W. Liu, Z. Fang, L. Zhou, T. J. Cui, *Adv. Opt. Mater.* **2015**, DOI: 10.1002/adom.201500156.

[51] L. H. Gao, Q. Cheng, J. Yang, S. J. Ma, J. Zhao, S. Liu, H. B. Chen, Q. He, W. X. Jiang, H. F. Ma, Q. Y. Wen, L. J. Liang, B. B. Jin, W. W. Liu, L. Zhou, J. Q. Yao, P. H. Wu, T. J. Cui, *Light: Sci. Appl.* **2015**, *4*, e324.
[52] P. Pitchappa, C. P. Ho, Y. Qian, Y. S. Lin, N. Singh, C. Lee presented at *IEEE 28th Int. Conf. on Micro Electro Mechanical Systems (MEMS)*, Estoril, January **2015**.
[53] Y. Qian, L. Lou, J. M. L. Tsai, C. Lee, *Appl. Phys. Lett.* **2012**, *100*, 113102.
[54] P. Singh, C. G. Li, P. Pitchappa, C. Lee, *IEEE Electron Device Lett.* **2013**, *34*, 8.
[55] B. W. Soon, E. J. Ng, V. A. Hong, Y. Yang, C. H. Ahn, Y. Qian, T. W. Kenny, C. Lee, *J. Microelectromech. Syst.* **2014**, *23*, 5.